


Nanocomposite SAC solders: morphology, electrical and mechanical properties of Sn–3.8Ag–0.7Cu solders by adding Co nanoparticles

A. Yakymovych^{1,2} · Yu. Plevachuk² · P. Švec Sr.³ · D. Janičkovič³ · P. Šebo⁴ ·
N. Beronská⁴ · M. Nosko⁴ · L. Orovcik⁴ · A. Roshanghias⁵ · H. Ipser¹ 

Received: 5 October 2016 / Accepted: 30 March 2017 / Published online: 8 April 2017
© The Author(s) 2017. This article is an open access publication

Abstract The effect of nanosized Co admixtures on the microstructure and physical properties of Sn–3.8Ag–0.7Cu solder and corresponding solder joints was investigated. The composite Sn–3.8Ag–0.7Cu ribbons with minor additions of Co nanoparticles (up to 1.0 wt%) were fabricated using the conventional planar flow casting method. The structure of nanostructured alloys was studied by X-ray diffraction and transmission electron microscopy. The electrical resistivity of Sn–3.8Ag–0.7Cu ribbons doped with nanoCo was measured by the standard four-point method. The microstructure and mechanical properties of corresponding solder joints (with Cu as substrate) were studied. It was shown that nanoCo additions led to minor changes in the electrical resistivity of Sn–3.8Ag–0.7Cu solder ribbons, while the nanoCo doped Sn–3.8Ag–0.7Cu solder joints (up to 0.5 wt% Co) revealed the reinforced microstructure accompanied by enhanced mechanical properties.

1 Introduction

In the recent past, the development of new solder materials based on ternary Sn–Ag–Cu (SAC) alloys has frequently focused on minor additions of ceramic or carbon nanoparticles as well as of transition metals in bulk and nanosized forms (Co, Fe, Mn, Ni, etc.). A large number of research and review papers described the impact of dopants on the microstructure and physical properties of SAC solders in the liquid and/or solid state [1–20]. It was shown that minor insertions of additional elements modify the microstructure and improve different properties of SAC alloys. For instance, the authors of Refs. [6, 9–11] pointed out that additional Co, Ni or Zn atoms substituted Cu atoms in the Cu₆Sn₅ phase and suppressed the formation of the brittle Ag₃Sn phase. Such structural changes improve both the microstructure and the mechanical properties such as microhardness and shear strength of doped SAC solders and their joints. However, it should be noted that in recent times the most popular way to reinforce SAC solders was the addition of ceramic nanoparticles into the SAC solder paste simply by mechanical mixing or by using the roll bonding procedure [12–17]. These minor (up to 1 wt%) additions of ceramic nanoparticles, such as Al₂O₃, TiO₂, ZrO₂, etc., improve the microstructure and mechanical properties of solder joints. Furthermore, the roll bonding method permits to achieve uniformly dispersed intermetallic compounds (IMCs) in the solder matrix by crushing brittle Ag₃Sn and Cu₆Sn₅ IMC crystals during the rolling process. Moreover, a recent study of nanocomposite SAC solders containing alumina nanoparticles coated with 0.1 wt% Ni and prepared by melt spinning showed a clear reduction in the growth of IMCs [21].

It appears that Co is one of the most frequently investigated nanosized metal admixtures added to lead-free SAC

✉ A. Yakymovych
andriy.yakymovych@univie.ac.at

¹ Department of Inorganic Chemistry – Functional Materials, University of Vienna, Althanstraße 14, 1090 Vienna, Austria

² Department of Metal Physics, Ivan Franko National University of Lviv, Lviv 79005, Ukraine

³ Institute of Physics, Slovak Academy of Sciences, Bratislava 84511, Slovakia

⁴ Institute of Materials and Machine Mechanics, Slovak Academy of Sciences, Bratislava 84513, Slovakia

⁵ CTR Carinthian Tech Research, 9524 Villach, Austria

solders. This fact is caused by a significant impact of minor amounts of nanoCo on the microstructure and physico-mechanical properties of the solder matrix and the SAC/Cu joint [2, 7, 18–20]. For instance, minor nanoCo additions increased the wetting angle and decreased the spreading rate of SAC solder [2]. It was shown that the microhardness of the composite solder increased slightly with the addition of Co nanoparticles [2, 7]. Additions of Co nanoparticles affected the morphology of SAC/Cu joints after reflow and aging processes. In particular, the interfacial morphology of SAC-nanoCo/Cu joints changed from a scallop to a more planar type, and the Cu_3Sn IMC tended to be suppressed during high temperature aging [2, 18, 19]. Another possibility is to mix nanoparticles with the flux [20]: incorporation of the metal nanoparticles (Co, Mo, Ni and Ti) into the flux affected the morphology and thickness of the interfacial IMC at the solder/substrate interface and also the wetting characteristics of the solder.

To our knowledge, the conventional planar flow casting method has not been applied to date to fabricate SAC based solders with nano-sized metal admixtures; up to now, Co nanoparticles were mainly mechanically mixed into SAC solder pastes. Therefore, the present study was dedicated to the suitability of the method for fabrication of nanocomposite SAC solders in the ribbon form as well as to the effect of nanosized Co admixtures on the electrical resistivity of Sn–3.8Ag–0.7Cu (wt%) (from now on SAC387) solder. Furthermore, the microstructure of SAC387-nanoCo/Cu joints after reflow was analyzed and the average thickness of IMC layers at the interface solder/Cu was estimated for the investigated joints. Additionally, the shear strength and microhardness of the SAC387-nanoCo/Cu joints were investigated.

2 Materials and methods

The SAC387 alloy used as master alloy in the present study was prepared from silver casting grains (99.9% metallic purity), tin ingot (99.998% metallic purity) and copper rod (99.9% metallic purity, all metals from Alfa Aesar, Karlsruhe, Germany). The samples were prepared by heating up to 1173 K accurately weighed amounts of pure components (within ± 0.1 mg) in evacuated and sealed quartz ampoules, and further aging at this temperature during 2 weeks.

The composite $(\text{SAC387})_{100-x}(\text{nanoCo})_x$ alloys were prepared by mixing SAC387 alloy with nominally 0.1, 0.3, 0.5 and 1.0 wt% Co nanoparticles (~ 28 nm, 99.8%, IOLITEC GmbH, Heilbronn, Germany). Mechanical dispersion of nanoparticles in the master alloy was achieved by manual stirring of Co nanoparticles in the SAC387 alloy for approximately 2–3 min at about 500 K. All

operations with Co nanoparticles were performed in a glove box (M. Braun, LabMaster 130) under the atmosphere of purified Ar (O_2 and $\text{H}_2\text{O} < 5$ ppm each).

The powder XRD patterns were measured on a Bruker D8 diffractometer at ambient temperature using Ni filtered CuK_α radiation (accelerating voltage 40 kV, electron current 40 mA). The diffractometer operated in the $\theta/2\theta$ mode. The powder was fixed with petroleum jelly on a single crystal silicon sample carrier, which was rotated during the measurement. A Lynxeye strip detector was used as a detection unit. Indexing of the phases was supported by the Inorganic Crystal Structural Database (ICSD). Rietveld refinement of the XRD patterns was done with the Topas3[®] software provided by Bruker AXS.

Polycrystalline ribbons ($6.6 \times 10^{-3} \times 2.0 \times 10^{-5} \times \text{m}$) were produced by the planar flow casting (PFC) technique at a temperature of about 50 K above the melting temperature of pure Sn (~ 505 K) for few seconds on air with an estimated cooling rate of 10^6 K s^{-1} . As an example, Fig. 1 shows the shape of the $(\text{SAC387})_{99.5}(\text{nanoCo})_{0.5}$ ribbon obtained using a binocular reflected light microscope (Zeiss Axiotech 100).

The structure of the polycrystalline ribbons was analyzed by transmission electron microscopy (TEM) using a conventional JEOL 2000FX at 200 kV. The nanocomposite ribbons were investigated on a Cu grid coated with a carbon film. The images were taken in bright and dark field to identify the Co nanoparticles in the SAC387 ribbon.

The electrical resistivity measurements were performed on air using a four-probe method with a continuous heating/cooling rate of 5 K min^{-1} . During these measurements, the samples were heated from room temperature up to about 630 K using a planar furnace. The temperature dependence of the electrical resistivity was monitored in terms of the relative electrical resistivity [standardized ratio $R(T)/R(T_0 = 300 \text{ K})$ in air atmosphere]. All details of the measurement techniques can be found elsewhere [22].

The solder ribbons obtained by planar flow casting were used to produce solder joints: four pieces of the same ribbon, inserted one on top of each other, were placed between two circular copper plates with diameters

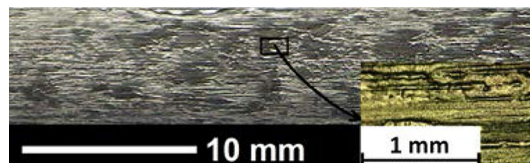


Fig. 1 The shape of the as-solidified $(\text{SAC387})_{99.5}(\text{nanoCo})_{0.5}$ ribbon

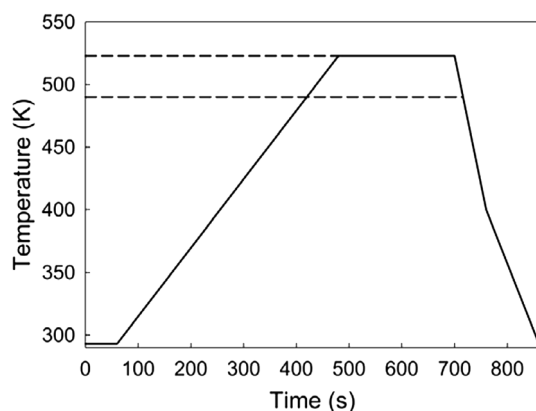


Fig. 2 Reflow temperature profile of solder/Cu joint

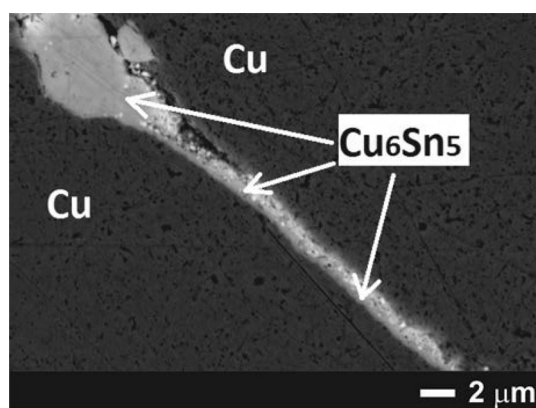


Fig. 3 SEM micrographs (BEI) of as-solidified solder joints made from SAC387 ribbon

of 1.0×10^{-2} and 1.5×10^{-2} m, respectively. The Cu/solder/Cu joints were prepared in an electric resistance furnace at the temperature of 523 K for 300 s in air atmosphere (Fig. 2). Cross-sectional specimens were prepared from the solders by standard metallographic technique. It should also be noted that the procedure of using four pieces of the solder ribbon between the Cu plates to make a joint was selected for practical reasons: with the use of just one piece in between the Cu plates the solder transformed into one single IMCs layer during reflow (Fig. 3).

An electron microscope JEOL 7600F was used for metallographic investigations. The excitation energy of the electron beam was 15–20 kV; backscattered electrons were detected in order to visualize the surfaces of the samples. The chemical analysis of the sample phases was performed using the energy dispersive X-ray technique (Oxford Instruments 50 mm² XMax silicon drift EDX) with the four characteristic spectral lines: K-line for Co, Cu and L-line for Ag, Sn. Standard deviations for the chemical compositions obtained from EDX were about ± 1 at.%. The average

thickness of the IMCs at the interface solder/Cu was calculated using the free software Digimizer which divided the area of the IMC layer by its length.

The shear strength of the joints was measured by a push-off method (Zwick/Roell Z 100) employing a loading rate of 1×10^{-3} m min⁻¹. The microhardness tests were performed using a Microhardness Tester FM-100. The square-based pyramidal diamond was pressed using a force of 0.049 N for a loading time of 10 s. The small area of the Vickers indentation tests made it possible to carry out a survey across the as-solidified joint. In our measurements, eight areas across each joint were tested to find an average value.

3 Results and discussion

3.1 Characterization of the SAC387 solder doped by Co nanoparticles

X-ray diffraction (XRD) was performed for as-synthesized composite SAC387-nanoCo alloys to check that Co nanoparticles remained inside the alloy and did not react with the Sn-based matrix. Otherwise, CoSn₃ compounds should be formed during the mixing process. No traces of any Co-Sn compound were found in the pattern confirming that Co nanoparticles did not react to any appreciable extent with the semi-solid Sn-based SAC387 matrix during manual stirring.

Transmission electron microscopy (TEM) was used to confirm the evidence of nanosized Co particles in as-synthesized composite SAC387-nanoCo ribbons. For this reason, images were taken in two modes with bright and dark backgrounds facilitating the detection of Co nano-inclusions in the alloy.

For instance, the high-resolution TEM images of the (SAC387)_{99.0}(nano Co)_{1.0} ribbon performed both in bright and dark-field modes confirmed the presence of Co nanoparticles in the SAC387 ribbons (Fig. 4). Thus, the structure analysis confirmed that the PFC technique can be used to produce the nano-composite SAC ribbons.

3.2 Effect of Co nanoparticles on the electrical resistivity of the SAC387 solder ribbon

As seen in Fig. 5, a good agreement between heating and cooling curves was observed for the solid SAC387 alloy: the heating curve shows values within 5% lower than the cooling curve. Our experimental results are also in satisfactory agreement with literature data for a commercial SAC387 alloy provided by the company “Métaux blancs ouverts” [23] and a self-made SAC387 alloy [24]. Furthermore, the experimental value of the electrical

Fig. 4 TEM images of the (SAC387)_{99.0}(nanoCo)_{1.0} ribbon in bright-field (a) and dark-field (b) modes

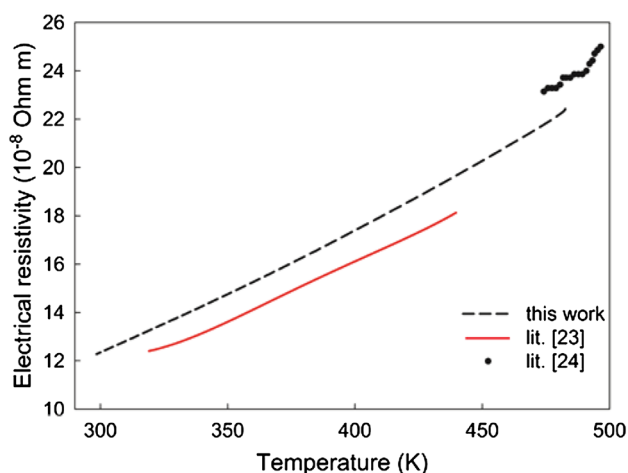
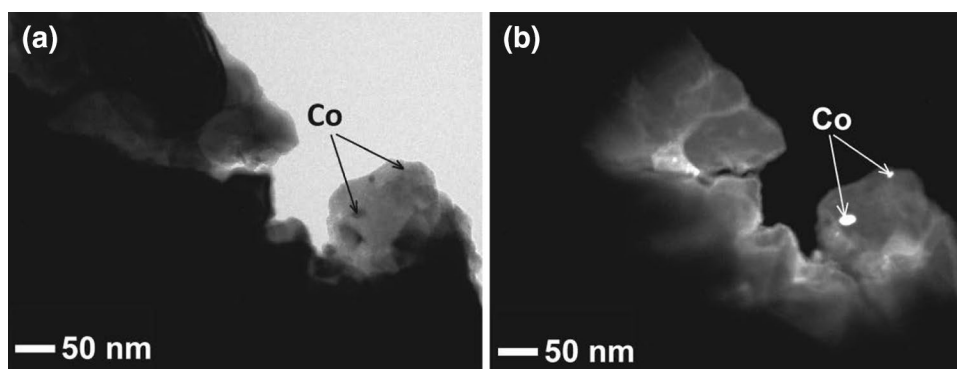


Fig. 5 Temperature dependence of the electrical resistivity for the SAC387 alloy

resistivity of the SAC387 solder at room temperature [$\rho(T_R) = 12.2 \times 10^{-8}$ Ohm m] is insignificantly lower than the recommended value for commercial SAC387 solders, which is equal to 13×10^{-8} Ohm m [25].

As mentioned above, the samples were overheated to about 630 K. It is suggested that during the first experimental run the electrical resistivity, $\rho(T)$, was actually measured in two different states: the first heating corresponds to the composite SAC387 solders with nanosized Co inclusions; however, at higher temperatures, i.e., around 490 K, the nanosized Co particles should be dissolved in the Sn-based matrix. According to Ref. [26], the melting temperature of nanocomposite (SAC305)_{100-x}(nanoCo)_x alloys up to 0.8 wt% nano Co is about 490 ± 1 K, which is in agreement with our assumption. Therefore, starting from the first cooling the electrical resistivity of quaternary (SAC387)_{100-x}Co_x alloys was actually measured. Based on that, the temperature dependence of the electrical resistivity for SAC387 ribbons with Co additions in bulk and nano-sized form was investigated (Fig. 6). The increase in the electrical resistivity with temperature for all investigated alloys can be approximated by the following polynomial,

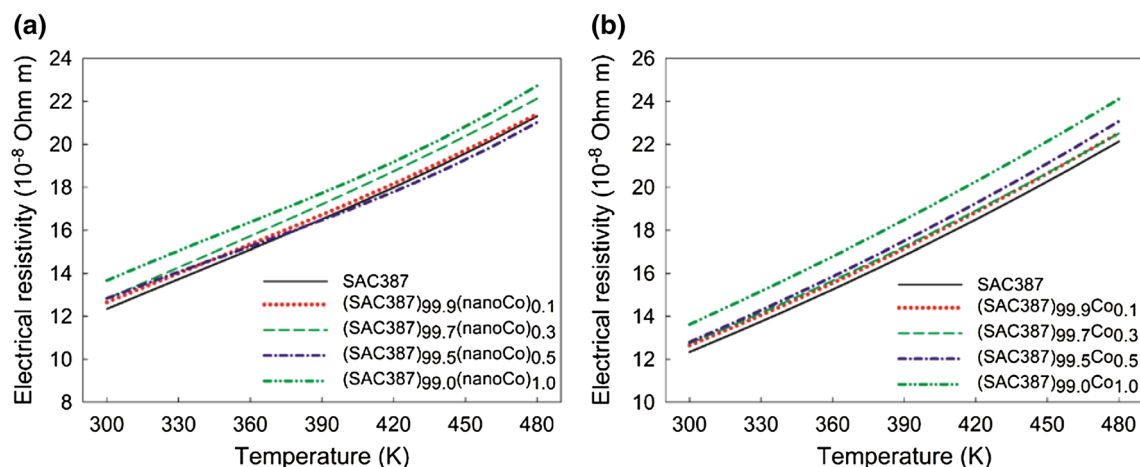


Fig. 6 Temperature dependencies of the electrical resistivity for (SAC387)_{100x}(nanoCo)_x ribbons: **a** heating; **b** cooling

$$\rho = A + B_1T + B_2T^2 + B_3T^3, \quad (1)$$

where A , B_1 , B_2 and B_3 are fitting coefficients; T is the temperature in Kelvin (with the coefficients presented in Table 1).

As seen in Fig. 6, small additions of Co up to 0.5 wt% led to insignificant changes in the electrical resistivity of the SAC387 alloy. An increase of the nanoCo amount up to 1.0 wt% led to an increase of the electrical resistivity of the SAC387 alloy, both in the original form (Fig. 6a) as well as after dissolution of the Co nanoparticles (Fig. 6b). This behavior complies with expected effects of solid solution alloying according to the Linde–Norbury rule [27]. According to this rule the effect of a solute on the electrical resistivity of a solvent is caused by an additional lattice-scattering term, which should be proportional to the square of the valence difference between applied solute and solvent. It

means that, to a first approximation, Co admixtures should have a less pronounced effect on the electrical resistivity of β Sn compared to Ag and Cu. Therefore, according to the Linde–Norbury rule, minor additions of Co should have a comparatively insignificant effect on the electrical resistivity of Sn. It should be noted that Co practically does not dissolve in pure Sn [28] while Co atoms substitute Cu in the Cu_6Sn_5 compound and vice versa Cu atoms substitute Co in the CoSn_3 compound [26]. Furthermore, the presented electrical resistivity values for $(\text{SAC387})_{100x}(\text{nanoCo})_x$ solder ribbons are in agreement with results from Ref. [29], where it was suggested that small amounts of a fourth element added to the SAC alloy (in the order of 0.5 at.% or less) causes only minor changes in the electrical resistivity of SAC-X solder joints (where X=Co, Fe and Bi).

The difference in the electrical resistivity values of quaternary SAC387-Co alloys obtained during first

Table 1 Fitting parameters of Eq. (1) for nanocomposite solders on first heating and for quaternary solders on first cooling

Sample (wt%)	A (10^{-8} Ohm m)	B_1 (10^{-10} Ohm m K^{-1})	B_2 (10^{-13} Ohm m K^{-2})	B_3 (10^{-16} Ohm m K^{-3})
First heating				
SAC387	−10.89	13.02	−25.00	24.67
$(\text{SAC387})_{99.9}(\text{nanoCo})_{0.1}$	−9.40	12.25	−23.29	23.21
$(\text{SAC387})_{99.7}(\text{nanoCo})_{0.3}$	−8.72	11.20	−19.16	19.20
$(\text{SAC387})_{99.5}(\text{nanoCo})_{0.5}$	−18.20	20.52	−47.56	45.48
$(\text{SAC387})_{99.0}(\text{nanoCo})_{1.0}$	−21.19	22.96	−52.85	50.16
First cooling				
SAC387	1.10	3.25	0.49	3.89
$(\text{SAC387})_{99.9}\text{Co}_{0.1}$	3.71	1.49	4.80	0.54
$(\text{SAC387})_{99.7}\text{Co}_{0.3}$	3.49	1.60	5.02	−0.19
$(\text{SAC387})_{99.5}\text{Co}_{0.5}$	0.22	4.05	−1.21	5.60
$(\text{SAC387})_{99.0}\text{Co}_{1.0}$	0.77	3.90	0.06	4.05

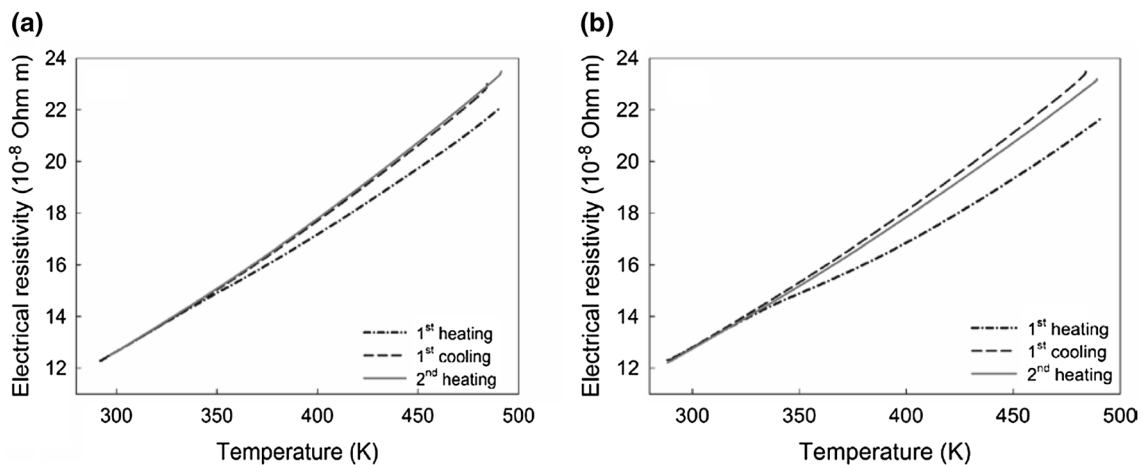


Fig. 7 Temperature dependence of the electrical resistivity for **a** $(\text{SAC387})_{99.9}(\text{nanoCo})_{0.1}$ alloy and **b** $(\text{SAC387})_{99.5}(\text{nanoCo})_{0.5}$ alloy

cooling and second heating does not exceed 5%. As seen in Fig. 7a, b, the $\rho(T)$ curves of (SAC387)_{99.9}Co_{0.1} and (SAC387)_{99.5}Co_{0.5} alloys corresponding to the second heating and the first cooling almost coincide.

Based on the presented data, it is suggested that minor additions of Co in nanosized form and as alloying element to SAC387 solders result in rather small changes in the electrical resistivity values (up to 7%). A similarly insignificant influence of metallic and ceramic nano-sized particles on the electrical resistivity of the solder Sn–3.5Ag and Sn–3.5Ag–0.7Cu matrix at ambient temperature was also found in Ref. [30]. The apparent increase in the electrical resistivity, observed for the alloy with 1 wt% Co addition, could be explained by microstructure changes related to an increase of Co-containing (Co,Cu)–Sn IMCs in the alloy.

3.3 Morphology and growth of interfacial IMCs layer at the interface solder/Cu

The cross sectional micrographs of the as-reflowed (SAC387)_{100x}(nanoCo)_x/Cu joints (with $x=0; 0.1; 0.3; 0.5$; and 1.0 wt%) are shown in Fig. 8. The intermetallic compound Cu₆Sn₅ formed the typical scallop type grains at the SAC387/Cu interface extending into the solder matrix (Fig. 8a). This discontinuous scallop-type IMC layer is caused by a rapid dissolution of Cu atoms from the substrate into the molten solder [31]. Visually discovered black points within the IMC layer correspond to Kirkendall voids formed in the Cu–Cu₃Sn and Cu₃Sn–Cu₆Sn₅ interfaces. A line-scan analysis of the SAC387/Cu joint confirmed the presence of a thin Cu₃Sn layer of about $0.3\text{ }\mu\text{m}$ at the interface zone (Fig. 9), while the calculated average thickness of the entire Cu₆Sn₅/Cu₃Sn layer at the interface was about $3.6\text{ }\mu\text{m}$ (Table 2). This is in agreement with our recent studies of the Cu₃Sn/Cu₆Sn₅ IMCs layer at the interface of SAC305/Cu solder joints [32].

Fig. 8 SEM micrographs (BEI) of as-solidified solder joints made from **a** SAC387; **b** (SAC387)_{99.9}(nanoCo)_{0.1}; **c** (SAC387)_{99.7}(nanoCo)_{0.3}; **d** (SAC387)_{99.5}(nanoCo)_{0.5}; **e**, **f** (SAC387)_{99.0}(nanoCo)_{1.0}

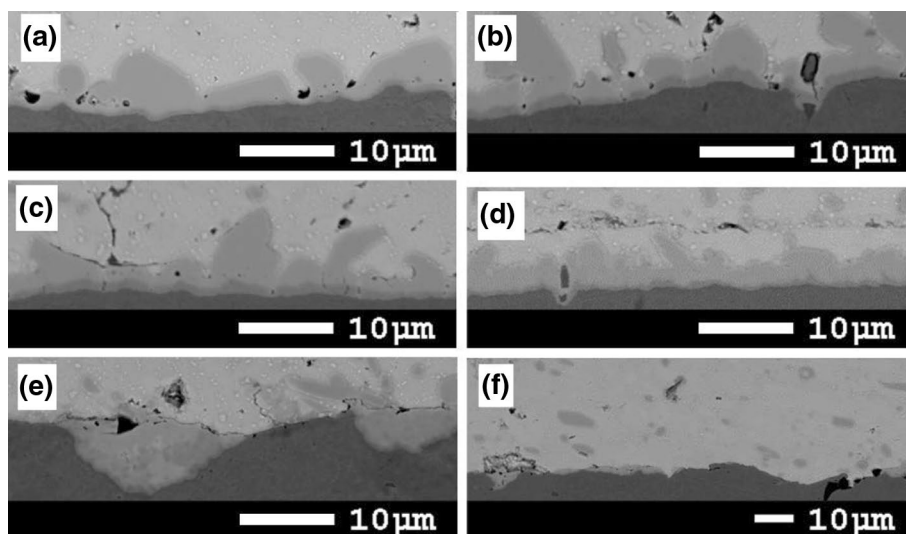


Fig. 9 SEM micrograph of an as-solidified SAC387/Cu solder joint together with the corresponding concentration profiles for Ag (green), Cu (red) and Sn (blue) across interface and matrix by EDX line scanning. (Color figure online)

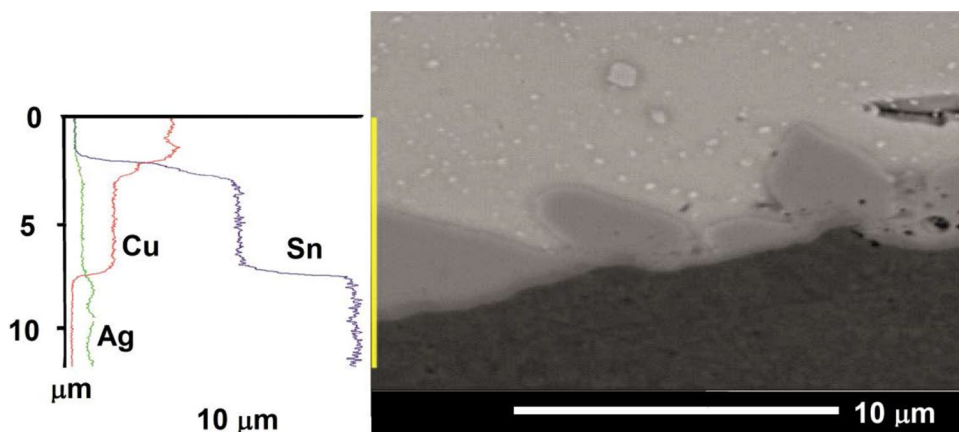


Table 2 The total average thickness of IMC layers at the interface solder/Cu

Solder (wt%)	Total average thickness of IMCs layer (μm)	
	$\text{Cu}_3\text{Sn} + \text{Cu}_6\text{Sn}_5 + (\text{Co,Cu})_6\text{Sn}_5$	Cu_3Sn
SAC387/Cu	3.3 ± 0.5	0.3 ± 0.1
(SAC387) _{99.9} Co _{0.1} /Cu	4.3 ± 0.5	1.0 ± 0.3
(SAC387) _{99.7} Co _{0.3} /Cu	4.8 ± 0.5	1.0 ± 0.3
(SAC387) _{99.5} Co _{0.5} /Cu	3.8 ± 0.4	0.7 ± 0.1

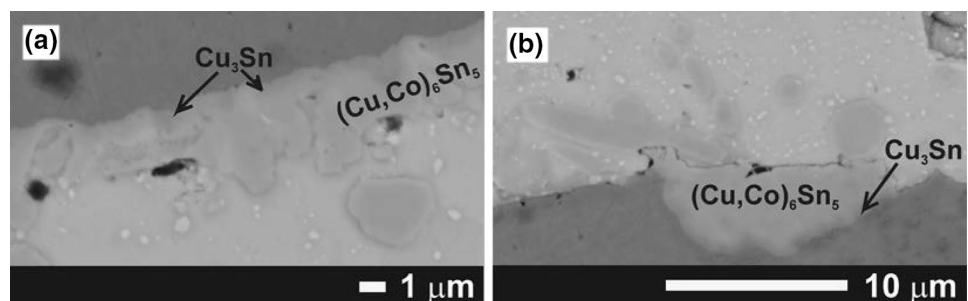
Addition of nanoCo leads to substantial changes in the morphology of the IMC layer at the interface (Fig. 8b–e). The influence of Co nanoparticles on the growth of the interfacial IMC layers was also examined by estimating the total average thickness of this $\text{Cu}_6\text{Sn}_5/\text{Cu}_3\text{Sn}$ layer for the investigated solder/Cu joints (Table 2). The addition of 0.1 wt% nanoCo led to an increase of the thickness of both Cu_6Sn_5 and Cu_3Sn IMC layers with a transition from a discontinuous to a more continuous scallop-type form (Fig. 8b). With the presence of 0.3 wt% of nanoCo in the SAC387 solder, the morphology of the IMC layer started to change to a more planar shape (Fig. 8c). A more or less planar-type IMC layer at the interface solder/Cu was indicated for a solder with 0.5 wt% of nanoCo (Fig. 8d). At the same time, a decrease in the thickness of the Cu_6Sn_5 and Cu_3Sn IMC layers could be observed for the solder joint with 0.5 wt% nanoCo compared to those for joints with 0.1 and 0.3 wt% of nanoCo (Table 2). Further increase of the nanoCo content up to 1.0 wt% led to a disappearance of the continuous IMC layer. Instead, IMCs “islands” were formed at the interface solder/Cu (Fig. 8e, f). Due to these dramatic changes in the morphology it was practically impossible to estimate the average thickness of IMCs along the interface. The presented results are in agreement with previous studies that reported a transformation of the interface IMC layer due to the addition of nano-sized Co forming $(\text{Co,Cu})_6\text{Sn}_5$ IMCs [18, 19, 33]. Furthermore, provided phase analysis for small areas on the SEM micrographs showed an evidence of Co both at the surface of IMCs layer and inside those for (SAC387)-(nanoCo)/Cu solder joints (Fig. 10).

The presented results indicate that nanoCo reinforcements affected the total average thickness and the morphology of the $\text{Cu}_6\text{Sn}_5/\text{Cu}_3\text{Sn}$ IMC layers at the interface of SAC387/Cu joints. The nature of these changes suggests that Co atoms concentrated on the surface of the IMC layers, producing $(\text{Co,Cu})_6\text{Sn}_5$, which affected the shape of the IMC, whereas in the bulk solder the amount of Cu_6Sn_5 increased with a simultaneous reduction in size. That these suggestions are in agreement with results of Refs. [26, 34] indicating a catalytic action of Co for the nucleation of solidification in SAC solders.

3.4 Effects of Co nanoparticles on mechanical properties of SAC387 solder joint

The shear strength values of Cu/solder/Cu joints for individual solders are given in Table 3. The shear strength of the joints increases continuously with increasing content of nanoCo (up to 0.3 wt%). As discussed above, the addition of 0.3 wt% of Co nanoparticles changes the shape and thickness of the interfacial IMC layer of the corresponding solder joint obviously resulting at the same time in an increase of the shear strength. Surprisingly, a further increase of the nanoCo content up to 0.5 wt% led to a decrease in the shear strength, although it was expected that formation of a more planar-type IMC layer on the interface, accompanied by an increase in the layer thickness, should lead to an increase of the shear strength. However, a closer examination of the SEM micrographs indicated also cracks initiating near the IMC layer and propagating along a significant part of the interface (Fig. 11). These cracks correspond to the IMC fracture mode [35] and should lead to the observed deterioration in the shear strength below those for unreinforced SAC387 solder. Excess addition of Co nanoparticles (up to 1.0 wt%) abruptly decreased the thickness of the $\text{Cu}_6\text{Sn}_5/(\text{Co,Cu})_6\text{Sn}_5/\text{Cu}_3\text{Sn}$ IMC layers at the interface resulting in a further decrease of the shear strength. A similar behavior of the shear strength for Sn–3.0Ag–0.5Cu/Cu solder joints with minor nanoCo additions (up to 1.0 wt%) was indicated in Ref. [2].

The microhardness of the solder joints increased slightly with the increase of the nanoCo content in the

Fig. 10 SEM micrograph of an as-solidified (SAC387)-(nanoCo)/Cu solder joint with 0.5 wt% (a) and 1.0 wt% Co (b)

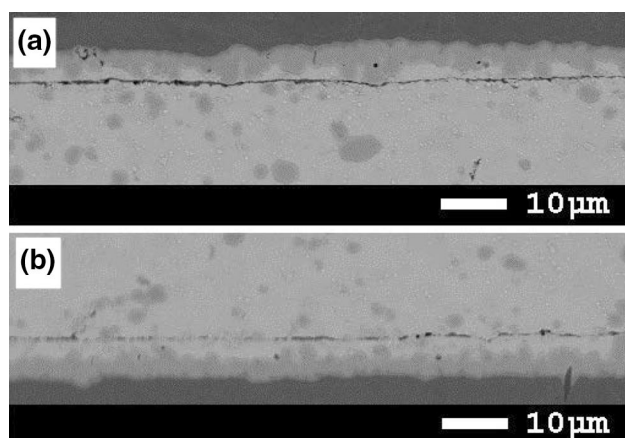


Fig. 11 SEM micrographs of as-solidified solder joints made from (SAC387)_{99.5}(nanoCo)_{0.5}/Cu joint on *top* (a) and *bottom* (b) parts

Table 3 The shear strength of (SAC387)_{100-x}Co_x/Cu solder joints

Solder (wt%)	Shear strength (MPa)
SAC387	13.6
(SAC387) _{99.9} Co _{0.1}	14.4
(SAC387) _{99.7} Co _{0.3}	15.6
(SAC387) _{99.5} Co _{0.5}	12.5
(SAC387) _{99.0} Co _{1.0}	10.6

(SAC387)_{100-x}Co_x/Cu solder joints from 19.8 VH for the SAC387 solder joint up to 21.5 VH for the joint with 0.5 wt%. The microhardness was equal 21.0 VH for the joint with 0.1 wt% Co and 21.3 VH for the joint with 0.3 wt% Co. This enhancement is contributed to the dispersion of refined IMC particles in the solder matrix where Co nano-inclusions acted as reinforcing centers. It is suggested, that the adsorption of Co nanoparticles on Cu₆Sn₅ IMC grains forming (Co,Cu)₆Sn₅ IMCs reduces the surface energy of the grains resulting in the suppression of Cu₆Sn₅ IMC growth and in an enhancement of the microhardness. Furthermore, the refinement of the microstructure could also be due to the formation of new (Co,Cu)Sn₃ IMC grains, the formation of which was also reported for (SAC305)_{100-x}Co_x (x = 0–0.8 wt%) alloys in Ref. [26].

4 Conclusions

In the present work the solder joints were produced and investigated using nanostructured SAC387 ribbons with nanoCo inclusions of up to 1.0 wt%. The morphology of the Cu–Sn IMC layers at the interface of the SAC387/Cu joints changed from a discontinuous to a more continuous

scallop-type shape with an addition of 0.3 wt% nanoCo resulting in an increase of the shear strength of the joints. Further additions of Co nanoparticles led to a practically full transition of the interface layer to a planar-type together with a decrease of the average thickness of IMC layers at the solder/Cu interface. However, the formation of cracks propagating along a significant part of the interface reduced the shear strength of the (SAC387)_{99.5}(nanoCo)_{0.5}/Cu connection. In contrast, the microstructure and microhardness of the bulk solder was continuously improved with further increases of nanoCo amounts up to 1.0 wt%. Such changes could be associated with the formation of (Co,Cu) Sn IMCs in the bulk solder and at the interface of the solder/Cu joints. Based on the present results it is suggested that SAC387 solders with 0.3 wt% of nanoCo in the ribbon form could be promising candidates for lead-free solder applications. It is also shown that minor additions of Co nanoparticles have an insignificant impact on the electrical resistivity of the SAC387 solder.

Acknowledgements Open access funding provided by Austrian Science Fund (FWF). This work was supported by the Slovak Scientific Grant Agency under Grant Numbers VEGA 2/0172/16 and VEGA 2/0189/14; the National Scholarship Program of the Slovak Republic; Austrian Science Fund (FWF) under Grant Numbers P 26304 and P 27049 and Ministry of Education and Science of Ukraine.

Open Access This article is distributed under the terms of the Creative Commons Attribution 4.0 International License (<http://creativecommons.org/licenses/by/4.0/>), which permits unrestricted use, distribution, and reproduction in any medium, provided you give appropriate credit to the original author(s) and the source, provide a link to the Creative Commons license, and indicate if changes were made.

References

1. I.E. Anderson, B.A. Cook, J. Harringa, R.L. Terpstra, J. Electron. Mater. **31**, 1166 (2002)
2. Y. Gu, Y. Liu, X.C. Zhao, S.L. Wen, H. Li, Y. Wang, Mater. Sci. Forum **815**, 97 (2015)
3. M.N. Bashir, A.S.M.A. Haseeb, A.M.S. Rahman, M.A. Fazal, C.R. Kao, J. Mater. Sci. **50**, 6748 (2015)
4. S. Chellvarajoo, M.Z. Abdullah, C.Y. Khor, Mater. Design **82**, 206 (2015)
5. D.A. Shnawah, S.B.M. Said, M.F.M. Sabri, I.A. Badruddin, F.X. Che, J. Electron. Mater. **41**, 2631 (2012)
6. A.K. Gain, Y.C. Chan, Intermetallics **29**, 48 (2012)
7. S.L. Tay, A.S.M.A. Haseeb, M.R. Johan, Solder Surf. Mt. Tech. **23**, 10 (2011)
8. H. Ma, J.C. Suhling, J. Mater. Sci. **44**, 1141 (2009)
9. K.S. Kim, K. Suganuma, 3rd international symposium on environmentally conscious design and inverse manufacturing: eco design 03, 414 2003
10. S.K. Kang, D.Y. Shih, D. Leonard, D.W. Henderson, T. Gosselein, S.I. Cho, J. Yu, W.K. Choi, JOM **56**, 34 (2004)
11. Y.W. Wang, Y.W. Lin, C.T. Tu, C.R. Kao, J. Alloy Compd. **478**, 121 (2009)

12. L.C. Tsao, R.W. Wu, T.H. Cheng, K.H. Fan, R.S. Chen, *Mater. Design* **50**, 774 (2013)
13. R. Kolenak, P. Sebo, M. Provaznik, M. Kolenakova, K. Ulrich, *Mater. Design* **32**, 3997 (2011)
14. T. Fouzder, Y.C. Chan, D.K. Chan, *J. Mater. Sci.* **25**, 5375 (2014)
15. Y. Tang, G.Y. Li, Y.C. Pan, *J. Alloy Compd.* **554**, 195 (2013)
16. Y. Tang, G.Y. Li, Y.C. Pan, *Mater. Design* **55**, 574 (2014)
17. A. Roshanghias, A.H. Kokabi, Y. Miyashita, Y. Mutoh, M. Rezayat, H.R. Madaah-Hosseini, *J. Mater. Sci.* **23**, 1698 (2012)
18. S.L. Tay, A.S.M.A. Haseeb, M.R. Johan, 12th electronics packaging technology conference, EPTC 2010, Singapore, 2010
19. A.S.M.A. Haseeb, T.S. Leng, *Intermetallics* **19**, 707 (2011)
20. G.K. Sujan, A.S.M.A. Haseeb, A.B.M. Afifi, *Mater. Charact.* **97**, 199 (2014)
21. K. Mehrabi, F. Khodabakhshi, E. Zareh, A. Shahbazkhan, A. Simchi, *J. Alloy Compd.* **688**, 143 (2016)
22. M. Deanko, M. Paluga, D.M. Kepaptsoglou, D. Muller, P. Mrafko, D. Janickovic, E. Hristoforou, I. Skorvanek, P. Svec, *J. Alloy Compd.* **434**, 248 (2007)
23. S. Mhiaooui, *Physical Properties of Lead Free Solders in Liquid and Solid State, Department of Physics*. (TU Chemnitz, Chemnitz, 2007), p. 165
24. W. Zhai, X. Zhao, X. Li, M. Fan, X. Xu, X. Wang, Z. Kang, W. Zhou, *J. Phys. Chem. Liq.* **54**, 37 (2016)
25. C. Schmetterer, H. Ipsen, J. Pearce, *ELFNET COST Action 531: Handbook of Properties of SAC Solders and Joints*. (Vydavatelství KNIHAR, Brno, Czech Republic, 2008)
26. A. Yakymovych, S. Mudry, I. Shtablavyi, H. Ipsen, *Mater. Chem. Phys.* **181**, 470 (2016)
27. P.L. Rossiter, *The Electrical Resistivity of Metals and Alloys* (Cambridge University Press, New York, 1987)
28. Y. Plevachuk, V. Sklyarchuk, I. Shtablavyi, S. Mudry, J. Brillo, H. Kobatake, A. Yakymovych, S. Fürtauer, B. Skolyszewska-Kühberger, K.W. Richter, H. Flandorfer, H. Ipsen, *J. Phys. Chem. Liq.* **54**, 440 (2016)
29. B.A. Cook, I.E. Anderson, J.L. Harringa, R.L. Terpstra, *J. Electron. Mater.* **31**, 1190 (2002)
30. P. Babaghorbani, S.M.L. Nai, M. Gupta, *J. Alloy Compd.* **478**, 458 (2009)
31. T. Laurila, V. Vuorinen, J.K. Kivilahti, *Mat. Sci. Eng. R* **49**, 1 (2005)
32. A. Yakymovych, Y. Plevachuk, P.S. Svec, P. Svec, D. Janickovic, P. Sebo, N. Beronska, A. Roshanghias, H. Ipsen, *J. Electron. Mater.* **45**, 6143 (2016)
33. M. Amagai, *Microelectron. Reliab* **48**, 1 (2008)
34. I.E. Anderson, J.C. Foley, B.A. Cook, J. Harringa, R.L. Terpstra, O. Unal, *J. Electron. Mater.* **30**, 1050 (2001)
35. K.E. Yazzie, H.E. Fei, H. Jiang, N. Chawla, *Acta Mater* **60**, 4336 (2012)